Ferrocene–Donor and 4,5-Dicyanoimidazole–Acceptor Moieties in Charge-Transfer Chromophores with π Linkers Tailored for Second-Order Nonlinear Optics

ARTICLE *in* CHEMISTRY - AN ASIAN JOURNAL · FEBRUARY 2013

Impact Factor: 4.59 · DOI: 10.1002/asia.201200963 · Source: PubMed

6 AUTHORS, INCLUDING:

Jirí Kulhánek
University of Pardubice
64 PUBLICATIONS **664** CITATIONS
SEE PROFILE

Filip Bureš
University of Pardubice
79 PUBLICATIONS **728** CITATIONS
SEE PROFILE

Wojciech Kuźnik
Czestochowa University of Technology
48 PUBLICATIONS **220** CITATIONS
SEE PROFILE

Iwan V Kityk
Czestochowa University of Technology
959 PUBLICATIONS **7,900** CITATIONS
SEE PROFILE

CHEMISTRY
AN ASIAN JOURNAL
ACES
FULL PAPER

DOI: 10.1002/asia.201200963

Ferrocene-Donor and 4,5-Dicyanoimidazole-Acceptor Moieties in Charge-Transfer Chromophores with π Linkers Tailored for Second-Order Nonlinear Optics

Jiří Kulhánek,[a] Filip Bureš,*[a] Wojciech Kuznik,[b] Iwan V. Kityk,[c] Tomáš Mikysek,[d] and Aleš Růžička[e]

Abstract: A series of new nonlinear optical chromophores (**1**–**15**) that were comprised of ferrocene-donor and 4,5-dicyanoimidazole-acceptor moieties and various π linkers of different length were synthesized. Support for the presence of significant D–A interactions in these NLO-phores was obtained from the evaluation of the quinoid character of the 1,4-phenylene moieties and their electronic absorption spectra, which featured intense high-energy (HE) bands that were accompanied by less-intense low-energy (LE) bands. The redox behavior of these compounds was investigated by cyclic voltammetry (CV) and by rotating-disc voltammetry (RDV); their electrochemical gaps decreased steadily from 2.64 to 2.09 V. In addition to the experimentally obtained data, DFT calculations of their absorption spectra, HOMO/LUMO levels, and second-order polarizabilities (β) (−2ω,ω,ω) were performed. A structure–property relationship study that was performed by systematically altering the π linker revealed that the intramolecular charge-transfer and nonlinear optical properties of these inorganic–organic hybrid D–π–A systems (**1**–**15**) were primarily affected by: 1) The presence of olefinic/acetylenic subunits; 2) the length of the π linker; and 3) the spatial arrangement (planarity) of the π linker.

Keywords: charge transfer · donor–acceptor systems · ferrocene · imidazole · nonlinear optics

Introduction

The growing area of molecular photonics and (opto)electronics continues to require new materials with improved and tailored nonlinear optical (NLO) properties. In this respect, organic molecules are very promising candidates, owing to their large optical nonlinearities and responses, their ease of synthesis, and their well-defined structures. Hence, an assortment of organic π-conjugated molecules are currently being investigated as active layers of (opto)electronic and data-storage devices, organic photovoltaic cells (OPVC), dye-sensitized solar cells (DSSC), (semi)conductors, organic light-emitting diodes (OLED), and switches.[1] A typical organic molecule that features optical nonlinearity consists of a π-conjugated scaffold that is end-capped by electron donors and acceptors. In such a D–π–A arrangement, efficient intramolecular charge transfer (ICT) from the donor to the acceptor takes place and the molecule becomes polarized (thereby constituting a dipole).[2] In this way, the polarization of the molecule in the strong electromagnetic field of a laser beam is facilitated and it possesses high first-order hyperpolarizability (β). Hence, the extent of ICT, which is primarily affected by the electronic behavior of the appended acceptors and donors, the length and structure of the π-conjugated system, and the overall planarity of the molecule, is responsible for the NLO response of the organic NLO-active chromophore (NLO-phore).[3] The active layers that are used in these devices usually consist of a polymeric matrix into which an NLO-phore is incorporated, either as a dopant (guest–host system) or as chemically bonded pendants (side-chain, main-chain, and cross-linked polymers). These types of arrangements further facilitate polarizability and improve thermal stability. The polar order of the resulting polymer (centrosymmetry removal) is most

[a] Prof. J. Kulhánek, Prof. F. Bureš
Institute of Organic Chemistry and Technology
Faculty of Chemical Technology, University of Pardubice
Pardubice, Studentská 573 (Czech Republic)
Fax: (+420) 46 603 7068
E-mail: filip.bures@upce.cz

[b] Dr. W. Kuznik
Physical Chemistry Department
Silesian University of Technology
Gliwice, Strzody 9, PL-44100 (Poland)

[c] Prof. I. V. Kityk
Electrical Engineering Department
Czestochowa University of Technology
Czestochowa, Armii Krajowej 17, PL-42201 (Poland)

[d] Dr. T. Mikysek
Department of Analytical Chemistry
Faculty of Chemical Technology, University of Pardubice
Pardubice, Studentská 573 (Czech Republic)

[e] Prof. A. Růžička
Department of General and Inorganic Chemistry
Faculty of Chemical Technology, University of Pardubice
Pardubice, Studentská 573 (Czech Republic)

Supporting information for this article is available on the WWW under http://dx.doi.org/10.1002/asia.201200963.

commonly achieved by applying an electric field or thermal (T_g or T_p) or optical-poling procedures.[4] In comparison to inorganic materials and despite the considerable progress in the development of new and functionalized push–pull systems, organic materials often suffer from low thermal stability and robustness. Hence, inorganic–organic hybrid systems could combine the advantages of both types of materials and constitute a very efficient NLO-phore. Over the last several years, we have focused on the design, synthesis, and application of organic push–pull systems that consist of aromatic backbones based on heterocycles, that is, imidazole and pyrazine.[5] A heteroaromatic moiety that is incorporated into the chromophore backbone strengthens its thermal and chemical robustness, whilst the heteroatoms may act as auxiliary electron donors or acceptors and further improve the intramolecular charge transfer and optical nonlinearity, respectively.[6]

Herein, we have linked a 4,5-dicyanoimidazole acceptor moiety to a ferrocene donor through a systematically varied and enlarged π-conjugated spacer. Ferrocene, with its unique electrical, magnetic, optical, redox, and crystal properties, as well as its high thermal and (photo)chemical stability, is a very useful building block in the construction of various functional materials[7] and has been used in numerous medicinal and bioorganometallic chemistry applications.[8] Since 1987,[9] ferrocene has also been recognized as an electron-donor moiety that is suitable for NLO-phores[10] and, subsequently, it has been utilized in push–pull systems of various designs and arrangements, such as D–π–A and D–π–D chromophores,[11–12] betaines,[13] Schiff bases,[14] and molecular wires.[15] Chromophores **1**–**15** represent inorganic–organic hybrid D–π–A systems in which heterocyclic acceptor units are connected to ferrocene donors through a π-conjugated system of double/triple bonds and 1,4-phenylene linkers. The fine-tuning of the optical, electrochemical, and NLO properties, as well as the spatial arrangement, of the NLO-phore was achieved by the extension and variation of the π linkers, which also allowed elucidation of the structure–property relationships.

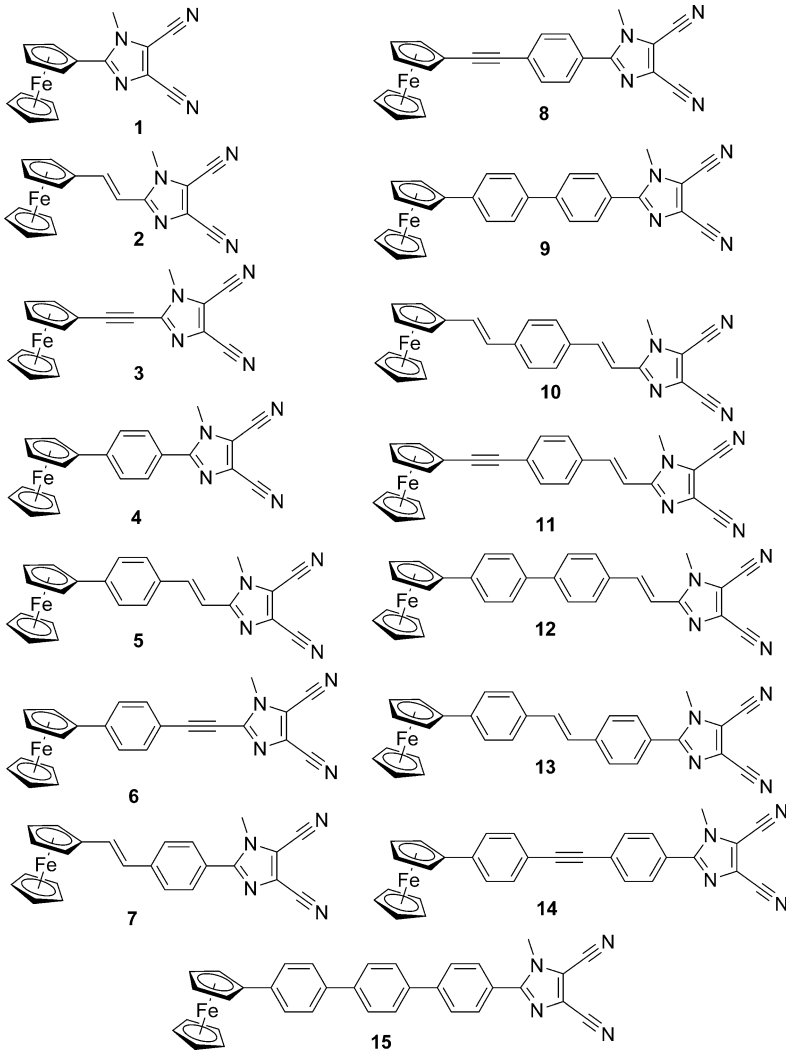

Abstract in Czech: Byla připravena série nových NLO chromoforů **1**–**15** obsahující ferrocen donorní a 4,5-dikyanoimidazol akceptorní části společně se systematicky prodlužovaným a měněným π-konjugovaným můstkem. Byla studována míra D-A interakce v těchto sloučeninách vyhodnocením chinoidního charakteru 1,4-fenylenových jednotek a absorpčních spekter vykazujících intenzivní vysokoenergetické (HE) pásy společně s nízkoenergetickými (LE) pásy o nižší intenzitě. Redoxní chování bylo zkoumáno pomocí cyklické voltametrie (CV) a rotačně-diskové voltametrie (RDV). Byl pozorován postupný pokles elektrochemického HOMO–LUMO rozdílu od 2.64 na 2.09 V. Tato experimentální data byla dále doplněna o DFT kalkulace absorpčních spekter, HOMO/LUMO hladin a polarizabilit druhého druhu (β) (−2ω,ω,ω) a předběžných SHG měření. Studium vztahů struktura-vlastnosti provedené systematickou obměnou π-konjugovaného můstku odhalilo, že vnitřní přenos náboje v anorganicko-organických hybridních D-π-A systémech **1**–**15** je především ovlivňován přítomností dvojných/trojných vazeb, délkou π-konjugované cesty a prostorovým uspořádáním můstku a jeho planaritou.

Results and Discussion

Synthesis

The synthesis of the target chromophores was accomplished by using Suzuki–Miyaura, Sonogashira, and Heck cross-coupling reactions, as shown in Scheme 1. Accordingly, 2-

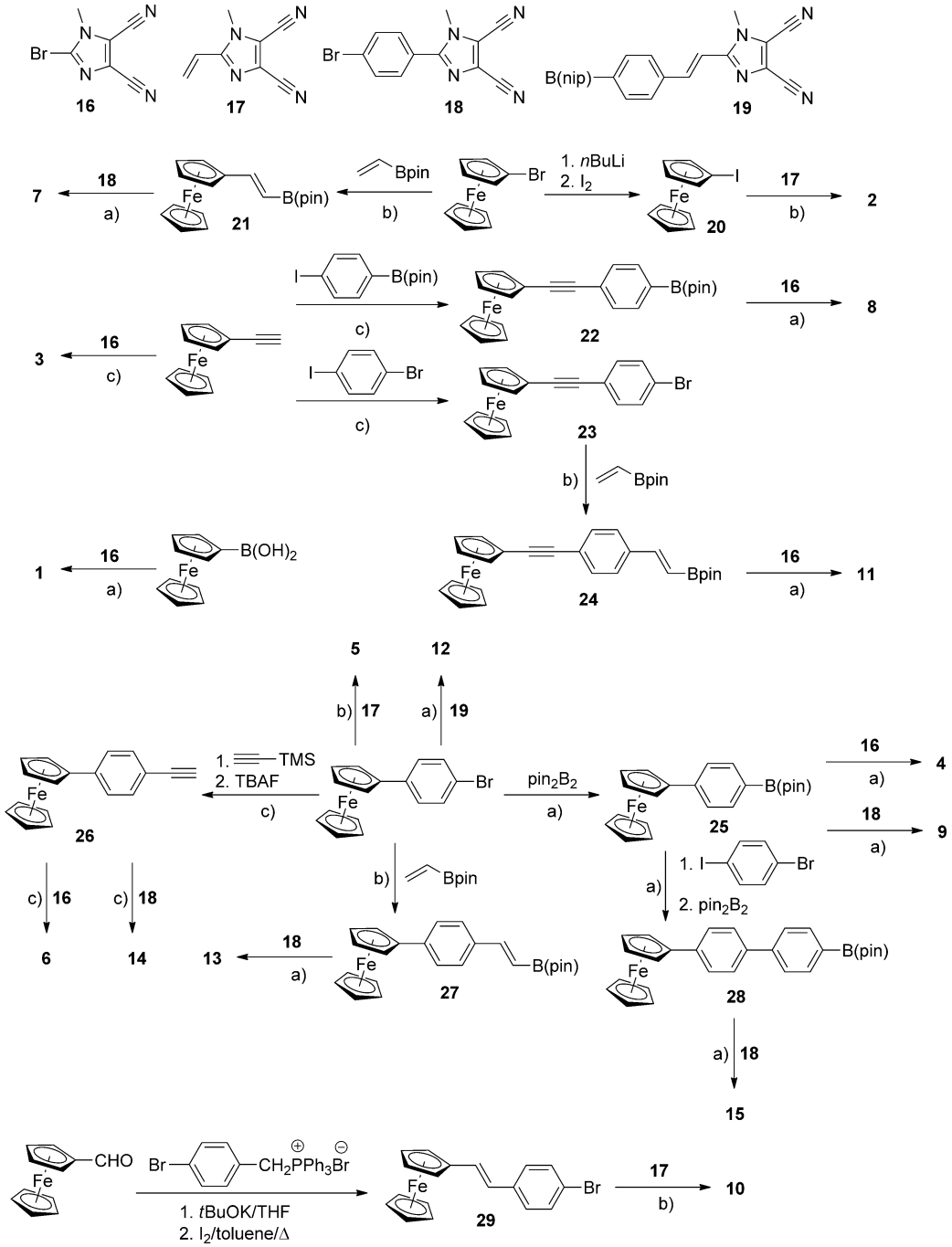

Scheme 1. General synthetic approach to π linkers **20**–**29** and NLO-phores **1**–**15**: a) Suzuki–Miyaura cross-coupling (Method A), $[PdCl_2(PPh_3)_2]$, Na_2CO_3, THF/H_2O (4:1), 80 °C; b) Heck olefination (Method B), $[Pd\{P(tBu)_3\}_2]$, iPr_2NH, DMF, 85 °C; c) Sonogashira cross-coupling (Method C), $[PdCl_2(PPh_3)_2]$, CuI, TEA, THF, 25 °C. TEA = triethylamine.

bromo-1-methylimidazole-4,5-dicarbonitrile (**16**),[5b,16] 1-methyl-2-vinylimidazole-4,5-dicarbonitrile (**17**, methylvinazene),[17] 2-(4-bromophenyl)-1-methylimidazole-4,5-dicarbonitrile (**18**), and boronic acid pinacol ester (**19**) were utilized as suitable precursors. Ferrocene-functionalized π linkers **20**–**29** were either commercially available or were synthesized from commercially available ferrocene, bromoferrocene, ethynylferrocene, ferrocenecarbaldehyde, and 4-bromophenylferrocene (all commercially available), as outlined in Scheme 1 and in the Supporting Information. Thus, bromoferrocene was converted into iodoferrocene (**20**, 71 %)[18] or treated with vinylboronate to afford compound **21** (24 %). Ethynylferrocene was utilized as a suitable terminal alkyne in Sonogashira reactions with 4-iodobenzeneboronic acid pinacol ester and 1-bromo-4-iodobenzene, thus providing compounds **22** and **23** in 67 and 72 % yield, respectively. This latter compound was treated with vinylboronate in a Heck reaction to yield π linker **24** (38 %). 4-Bromophenyl-

ferrocene, which was easily synthesized from ferrocene and 4-bromoaniline,[19] was used as an electrophile in the Suzuki–Miyaura, Sonogashira, and Heck cross-coupling reactions to yield intermediates **25** (52%), **26** (45%, including TMS-group removal), and **27** (41%), respectively. The selective cross-coupling of boronic acid pinacol ester **25** with 1-bromo-4-iodobenzene and subsequent treatment with bis(pinacolato)diboron afforded biphenyl-derived π linker **28** in 28% overall yield. 4-Bromostyrylferrocene **29** was synthesized in 66% yield from ferrocenecarbaldehyde and 4-bromobenzyltriphenylphosphonium bromide through a Wittig reaction followed by isomerization.

Bromoimidazole **16** was cross-coupled with ferroceneboronic acid, ethynylferrocene, and π linkers **22** and **24**–**26** to afford target chromophores **1** (21%), **3** (48%), **4** (72%), **6** (31%), **8** (62%), and **11** (55%). Methylvinazene (**17**) has recently been utilized as a fully planar electron-acceptor unit[20,5a] that can easily be cross-coupled with various electrophiles through Heck olefination. By using this reaction, 4-bromophenylferrocene and compounds **20** and **29** provided the target NLO-phores (compounds **5**, **2**, and **10**) in 65, 44, and 44% yield, respectively. The Suzuki–Miyaura and Sonogashira cross-coupling reactions of the remaining π linkers (compounds **21** and **25**–**28**) and 4-bromophenylferrocene with bromophenylimidazole **18** (which was synthesized from 4-bromobenzaldehyde and diaminomaleonitrile, DAMN)[21] and boronic acid ester **19** (for its synthesis, see reference [5e]) yielded chromophores **7** (41%), **9** (51%), **13** (65%), **14** (51%), **15** (51%), and **12** (69%).

X-ray Crystal Structures and Bond-Length Alternation

Target push–pull chromophores **1**, **5**, **6**, **8**, and **9** were crystallized by the slow evaporation of their solutions in $CDCl_3$ (which were used for the NMR measurements). Their crystal structures are shown in Figure 1 and in the Supporting Information (Table S1 and Figure S1–S5). Because the geometric and electronic parameters of organic π-conjugated molecules are closely related to one another,[22] the spatial arrangement of the donor and acceptor groups that are attached onto the central π linker, the overall planarity of the chromophore, and bond-length alternation (BLA)[23] are the most crucial structural features that affect D–A interactions in the ground state. The overall planarity of a chromophore can be quantified by its torsion angles (ϕ_1–ϕ_3) between the ferrocene Cp, 1,4-phenylene, and imidazole planes (Figure 1, Table 1). In contrast to the central π linkers in chromophores **1**, **5**, **6**, and **8** (phenylethenyl, phenylethynyl, and ethynylphenyl spacers), which could be considered to be planar, the two 1,4-phenylene moieties in chromophore **9** adopt a "propeller-like" structure with a torsion angle of $\phi_3 = 30.1°$ between the two 1,4-phenylene rings; this value is typical for biphenyl compounds.[24,5b] Whilst the Cp and imidazole rings are almost coplanar ($\phi_1 = 3.7°$) in the simplest chromophore (**1**), the donor–acceptor moieties in compound **5**, **6**, **8**, and **9** are twisted, owing to their attachment to the central π linker. In this respect, the insertion of ethenylene

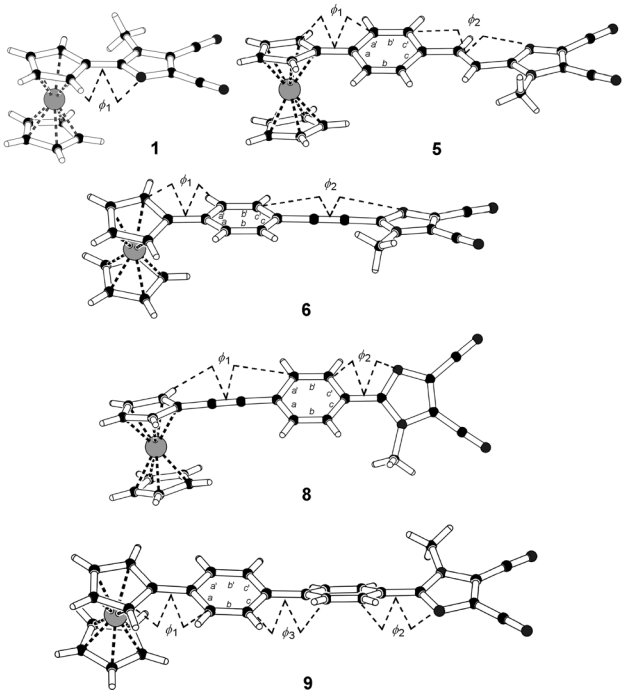

Figure 1. Single-crystal X-ray structures of NLO-phores **1**, **5**, **6**, **8**, and **9** at 150 K. CCDC 865751 (**1**), CCDC 865753 (**5**), CCDC 865755 (**6**), CCDC 865752 (**8**), and CCDC 865754 (**9**) contain the supplementary crystallographic data for this paper. These data can be obtained free of charge from The Cambridge Crystallographic Data Centre via www.ccdc.cam.ac.uk/data_request/cif.

Table 1. Structural features of chromophores **1**, **5**, **6**, **8**, and **9**, as obtained by RTG/DFT analysis.

Compound	ϕ_1 [°]	ϕ_2 [°]	ϕ_3 [°]	δr
1	3.7/23.5	–	–	–
5	15.2/13.8	2.2/5.6	–	0.018/0.025
6	21.9/10.4	2.0/0.3	–	0.014/0.027
8	7.3/3.3	31.4/28.9	–	0.018/0.026
9	10.6/8.4	30.9/34.0	30.1/29.5	0.018/0.019

or ethynylene subunits was shown to be very beneficial and caused partial planarization of the π-conjugated system, as in compounds **5** ($\phi_2 = 2.2°$), **6** ($\phi_2 = 2.0°$), and **8** ($\phi_1 = 7.3°$). The extent of D–A interaction was also evaluated by determining the degree of bond-length alternation in the 1,4-phenylene rings of chromophores **5**, **6**, **8**, and **9** (Table 1. These moieties featured almost-constant average quinoid character ($\delta r \approx 0.018$ Å), which resembles the values that were measured for D–A phenylacetylenes.[23a] Thus, all of the 1,4-phenylene rings in these chromophores are similarly polarized (benzene: $\delta r = 0.00$, fully quinoid structure: $\delta r =$ 0.10–0.12). Furthermore, these aforementioned RTG-derived data were compared to their DFT-calculated values, as shown in Table 1. The computational results showed similar deviation from planarity and BLA values as the experimental data. However, notably, the calculations were performed for isolated molecules in a vacuum.

Electrochemistry

Cyclic voltammetry (CV) and rotating-disc voltammetry (RDV) electrochemical measurements were carried out in DMF that contained 0.1 M Bu_4NPF_6 as the electrolyte in a three-electrode cell. The working electrode was a Pt disc (diameter: 2 mm). A saturated calomel electrode (SCE) and Pt wire, separated by a bridge that was filled with supporting electrolyte, were used as the reference and auxiliary electrodes, respectively. The acquired data are summarized in Table 2 and in the Supporting Information, Table S2. Representative CV curves for compounds **2**, **7**–**10**, and **15** are shown in the Supporting Information (Figure S6–S11). The half-wave potentials of the first oxidation and reductions were recalculated to afford standard reduction potentials E_{HOMO} and E_{LUMO}.[26] These potentials can be further correlated with the corresponding DFT-calculated HOMO and LUMO levels.

Whereas the first oxidation was likely localized on the ferrocene donor, the first reduction involved the 4,5-dicyanoimidazole acceptor moiety and the π linker. All of the studied chromophores showed one reversible one-electron oxidation with the first oxidation potential within the range +0.72 to +0.46 V. In contrast to the oxidation of similar alkoxy- or dialkylamino-donor-substituted chromophores,[5b] the first oxidation potential of compounds **1**–**15** was dependent on the structure and length of the π linker. Compared to the simplest chromophore (**1**, $E_{1/2(ox1)}=+0.67$ V), the first oxidation of chromophore **2** ($E_{1/2(ox1)}=+0.55$ V), which contained a double bond, was facilitated by the π-linker extension and planarization of the chromophore. In contrast, the insertion of the more electronegative ethynylene unit[2d,25] in compound **3** resulted in an increase in the first oxidation potential to +0.72 V. The "insulating" effect of the acetylenic subunit was also shown in the oxidation of chromophores **8** ($E_{1/2(ox1)}=+0.61$ V) and **11** ($E_{1/2(ox1)}=+0.61$ V). The insertion of an olefinic subunit between the donor–acceptor moieties and the central π linker, as in compounds **7** ($E_{1/2(ox1)}=+0.48$ V) and **12** ($E_{1/2(ox1)}=+0.50$ V), shifted the first oxidation potential to less-positive values by 100–200 mV. The beneficial effect of a "more transparent" olefinic subunit was the most pronounced in chromophore **10** (which contained a central 1,4-phenylene unit and the donor–acceptor moieties were linked through two additional double bonds), which was oxidized at the lowest potential (+0.46 V).

The first reduction was most likely localized on the 4,5-dicyanoimidazole acceptor moiety as a main reduction center, whereas subsequent reductions involved the π linker. The observed first reductions were one-electron and reversible processes that ranged from −1.97 to −1.55 V and were clearly dependent upon the length and structure of the π linker. Whereas the reduction of compound **1**, which possessed no additional π linker, occurred at −1.97 V, the reduction of chromophores **2**–**15**, with systematically enlarged π linkers, steadily decreased from −1.88 to −1.55 V. However, the position of the first reduction peak was also affected by the composition and spatial arrangement of the π linker. The "insulating" character of the acetylenic linker also affected the first reduction, as revealed by a comparison of structural analogues **2**/**3** and **7**/**8**. Whereas chromophores **3** ($E_{1/2(red1)}=-1.77$ V) and **8** ($E_{1/2(red1)}=-1.80$ V), which contained triple bonds, were reduced at more positive potentials as a result of the decreased electron transfer of electron density from the donor to the acceptor moieties, the first reduction potentials of chromophores **2** ($E_{1/2(red1)}=-1.88$ V) and **7** ($E_{1/2(red1)}=-1.85$ V), which featured "more transparent" olefinic subunits, were anodically shifted by 110 and 50 mV, respectively. Although chromophores **9** and **15** possessed two of the largest π linkers, the non-planar arrangement of the 1,4-phenylene subunits that were directly appended to the donor and acceptor moieties (see X-ray analysis, above) caused a substantial anodic shift of the first reduction potentials to −1.87 and −1.84 V, respectively. The lowest difference between the first oxidation and reduction potentials (HOMO–LUMO gap) was measured for fully planar chromophore **10** ($\Delta E=2.09$ V).

Table 2. Electrochemical data and optical properties of chromophores **1**–**15**.

Compound	$E_{1/2(ox1)}$ [V][a]	$E_{1/2(red1)}$ [V][a]	ΔE [V][b]	E_{HOMO} [V][c]	E_{LUMO} [V][c]	λ_{max}^{HE} [nm (eV)]/ ε ($\times 10^3$) [$M^{-1}cm^{-1}$]	λ_{max}^{LE} [nm (eV)]/ ε ($\times 10^3$) [$M^{-1}cm^{-1}$]
1	+0.67	−1.97	2.64	5.02	2.38	284(4.36)/13.4	453(2.74)/0.4
2	+0.55	−1.88	2.43	4.90	2.47	321(3.86)/25.6	484(2.56)/2.9
3	+0.72	−1.77	2.49	5.07	2.58	299(4.15)/17.8	457(2.71)/1.1
4	+0.55	−1.88	2.43	4.90	2.47	299(4.15)/22.1	463(2.68)/1.2
5	+0.52	−1.68	2.20	4.87	2.67	346(3.58)/34.9	472(2.63)/3.7
6	+0.54	−1.73	2.27	4.89	2.62	321(3.86)/31.8	465(2.67)/2.4
7	+0.48	−1.85	2.33	4.83	2.50	331(3.75)/29.1	471(2.63)/2.8
8	+0.61	−1.80	2.41	4.96	2.55	312(3.97)/27.9	448(2.77)/1.5
9	+0.50	−1.87	2.37	4.85	2.48	312(3.97)/33.6	446(2.78)/1.5
10	+0.46	−1.63	2.09	4.81	2.72	369(3.36)/37.8	474(2.62)/5.4
11	+0.61	−1.55	2.16	4.96	2.80	347(3.57)/42.3	465(2.67)/3.6[d]
12	+0.50	−1.63	2.13	4.85	2.72	349(3.55)/44.8	466(2.66)/2.6[d]
13	+0.50	−1.76	2.26	4.85	2.59	348(3.56)/41.9	462(2.68)/3.4[d]
14	+0.52	−1.76	2.28	4.87	2.59	328(3.78)/37.7	464(2.67)/2.1[d]
15	+0.49	−1.84	2.33	4.84	2.51	317(3.91)/45.4	462(2.68)/1.3[d]

[a] $E_{1/2(ox1)}$ and $E_{1/2(red1)}$ are the half-wave potentials of the first oxidation and reduction, respectively, as measured by RDV. [b] $\Delta E=E_{1/2(ox1)}-E_{1/2(red1)}$; the potentials are given versus SCE. [c] $E^{abs}_{HOMO/LUMO}=E_{1/2(ox1/red1)}+4.350$, see reference [26]. [d] Barely distinguishable shoulder.

UV/Vis Spectroscopy

In contrast to organic D–π–A chromophores, in which a single low-energy ICT transition is observed and determines the NLO response,[2,3] analogous NLO-phores that contain a metallocene donor moiety show two low-energy transitions. According to Marder and co-workers,[11i] the low-energy (LE) absorption could be attributed to a transition from the Fe-centered HOMO to the LUMO, which

was largely localized on the 4,5-dicyanoimidazole acceptor moiety and partially on an adjacent π linker (M→A). The higher-energy (HE) absorption originated from the interaction of the HOMO−3, which was localized on the Cp ring and the π linker, with the LUMO of the acceptor (π→A). This model predicted that an extension of the π-conjugated systems would lead to a red-shift of the HE transition, whilst only negligibly affecting the energy of the LE transition.

The selected absorption spectra of chromophores **1–3** and **7–10** in CH_2Cl_2 are shown in Figure 2; their full spectra are shown in the Supporting Information, Figures S17–S19 and

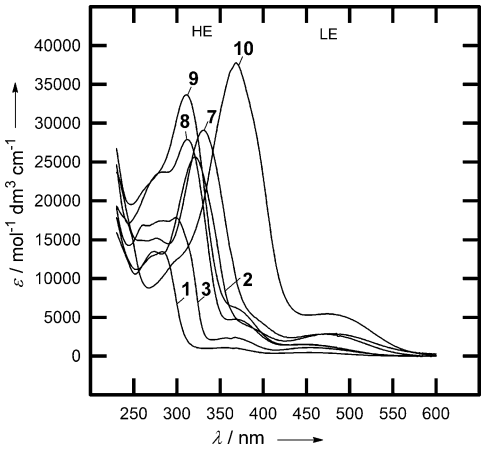

Figure 2. Selected UV/Vis spectra of chromophores **1–3** and **7–10** ($c = 2 \times 10^{-5}$ M in CH_2Cl_2).

the data are summarized in Table 2. The positions of the HE and LE absorption bands range from 284–369 and 453–484 nm, respectively. A comparison of compound **1** with compounds **2** and **3** clearly shows the influence of extension of the π-conjugated path by incorporating olefinic and acetylenic subunits. Whereas both units shifted the HE absorption bands bathochromically, by 37 and 15 nm, respectively, the position of the LE absorption band of compound **3** remained almost unchanged. In contrast, the LE absorption band of compound **2** was also shifted by 31 nm as a result of the presence of a "transparent" olefinic subunit. Similar behavior was observed in a comparison of chromophores **7** and **8**. The HE/LE bands for chromophore **9**, which contained an extended but twisted central biphenyl π linker, were in almost the same positions as those of chromophore **8**. The most red-shifted HE and LE absorption bands were measured for chromophore **10**, which corresponded to the aforementioned electrochemical behavior. Further extension of the π linker, as in compounds **11–15**, did not lead to a bathochromic shift of the HE/LE absorption bands. Hence, these data adhered to the model predicted by Marder and co-workers with the addition that the LE transitions were more pronounced if the π linker consisted of a polarizable/planar olefinic subunit.

The methoxy- and *N*,*N*-dimethylamino-substituted structural analogues of chromophores **1**, **4**, **5**, **9**, **13**, and **14** have also been synthesized recently;[5b] therefore, these compounds were also compared in this study. The first oxidation potentials of ferrocene-substituted chromophores are generally lower as a result of the presence of the easily oxidizable ferrocene donor; however, the observed first reduction potentials and the HOMO–LUMO gaps matched the trends that were observed for the methoxy- and *N*,*N*-dimethylamino-substituted analogues (see the Supporting Information, Figures S12 and S13). A comparison of the electrochemically measured HOMO–LUMO gaps (ΔE) for each series of compounds (see the Supporting Information, Figure S14) revealed that the smallest differences were for the ferrocene-substituted chromophores. This observation correlated with the positions of the low-energy CT bands (Fe-centered HOMO→LUMO interaction), for which the highest bathochromic shift was observed (see the Supporting Information, Figure S15). However, when considering the position of the high-energy CT bands (interaction of Cp-localized HOMO−3 to LUMO), the ferrocene-substituted chromophores showed ICT efficiency that lay between the methoxy- and *N*,*N*-dimethylamino-substituted analogues (see the Supporting Information, Figure S16). Hence, considering all of these data, ferrocene must be treated as a donor that shows dual ICT with different efficiencies.[27]

Calculations and NLO Properties

Chromophores **1–15** were also investigated theoretically by performing (TD)DFT calculations. The HOMO and LUMO energy levels and their optical gaps are presented in Table 3. The theoretically-derived LUMO energy levels and the optical energy gaps, which were calculated by using a hybrid B3LYP functional that took into account exchange-correlation effects, were very close to their corresponding experimental values, as measured by CV (Table 2), with an average error of 0.11 eV. Because this error is close to the precision of the experiment, this computational method can be considered to be a reliable tool for the orbital description of compounds **1–15**. Compared to the electrochemically measured energies of the HOMOs (Table 2), the DFT-derived values were slightly shifted to higher energies. However, the general trends in the E_{HOMO}, E_{LUMO}, and ΔE values as observed by DFT calculations resembled those from the electrochemical measurements. The global gradient approximation functional BLYP was also tested (see the Supporting Information, Table S3). However, as we had observed previously,[28] this method failed to properly describe the energy levels in the molecules, thereby underestimating the energy gaps by about 0.7 eV. A representative HOMO and LUMO (for chromophore **10**) are shown in Figure 3 (for a complete list, see the Supporting Information, Figures S66–S95). Whereas the HOMO was mainly localized on the ferrocene donor, the LUMO was placed on the 4,5-dicyanoimidazole acceptor moiety and was partially spread over the π linker. These results clearly confirmed the assumption that was deduced from the electrochemical measurements (see above).

Table 3. Computational and preliminary experimental results for chromophores **1**–**15**.

Compound	E_{HOMO} (DFT)[a]	E_{LUMO} (DFT)[a]	$\Delta E_{(optical)}$ (TDDFT)[a]	β (−2ω,ω,ω)[b]	Experimental SHG signal[c]	Dipole moment (μ) [D]		
						Ground state[d]	Vertically excited state[e]	Increase [%]
1	−4.77	−1.81	2.91	32	0	9.1	9.1	0
2	−6.08	−2.56	2.19	41	2.05 (701.5)	10.6	13.0	23
3	−6.22	−2.51	2.26	32	–	10.7	12.1	13
4	−5.97	−2.42	2.31	49	–	10.3	11.8	14
5	−5.89	−2.77	2.26	159	2.40 (1003.8)	11.2	15.5	38
6	−5.98	−2.69	2.26	128	–	11.8	15.2	28
7	−5.85	−2.55	2.25	131	–	11.3	14.5	29
8	−5.94	−2.57	2.28	111	–	10.7	13.1	22
9	−5.74	−2.86	2.30	155	–	10.7	12.1	13
10	−5.85	−2.90	2.20	393	3.14 (1395.1)	12.1	17.8	47
11	−5.85	−2.90	2.25	291	2.89 (1278.2)	11.5	16.6	45
12	−5.69	−2.72	2.28	396	–	11.1	15.0	34
13	−5.66	−2.58	2.29	290	2.13 (1053.0)	11.3	15.3	36
14	−5.73	−2.57	2.29	238	–	10.9	14.2	30
15	−5.72	−2.52	2.34	138	–	11.0	12.0	9

[a] In eV; ΔE calculations (TDDFT) were performed with the 6-31G(df,p) basis set; the HOMO and LUMO levels were calculated with the 6-311++G(3df,2dp) basis set, except for compounds **12**, **13**, and **14**, where 6-311G-(3df,2dp) was used; the B3LYP functional and PCM model (CH_2Cl_2) were used in all cases. [b] In cm^4/statvolt; ω = 1064 nm; CAM-B3LYP functional, 6-31+G(df,p) basis set, and PCM (polycarbonate: ε = 2.5, solvent radius: 12 nm) were used. [c] SHG signal of the sample that was embedded into a photopolymer (polycarbonate, 7.7–8.5 %), measured at 1064 nm. Only clearly distinguishable signals are presented. The values in parentheses are relative to the molecular mass of the chromophore. [d] DFT B3LYP with 6-311++G (3df,3pd) for compounds **1**–**11**/**15** and 6-311G(3df,3pd) for compounds **12**–**14**. [e] TDDFT B3LYP 6-31G(df,p).

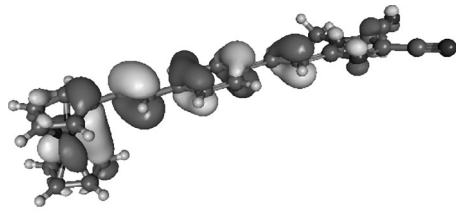

10 (HOMO, -5.85 eV)

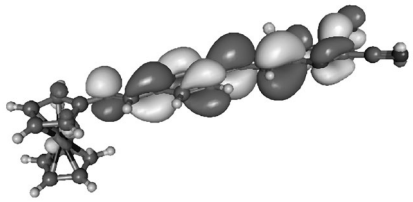

10 (LUMO, -2.90 eV)

Figure 3. Representative HOMO and LUMO localization in compound **10**.

The first nonzero optical transitions, such as in compound **10**, were accompanied by a significant charge transfer. The theoretically predicted absorption spectra for all of the tested chromophores (**1**–**15**) correlated reasonably well with those that were measured experimentally in CH_2Cl_2 (see the Supporting Information, Figures S62–S65).

The first-order hyperpolarizabilities (β) (−2ω,ω,ω) of these compounds at 1064 nm were theoretically calculated by using coupled-perturbed Hartree–Fock calculations with the CAM-B3LYP functional 6-31+G(df,p) basis set and the PCM model (polycarbonate: dielectric constant and solvent radius were arbitrarily set to 2.5 and 12 nm, respectively). The calculated values are shown in Table 3. The calculated second-order nonlinearities ranged from 32 to 396 cm^4/statvolt. More importantly, the calculated values exactly mirrored the trends that were observed by using the previously described analytical tools that were used to determine the extent of D–A interaction and molecule polarization. For instance, the beneficial role of the olefinic subunit can be demonstrated by a comparison of chromophores **4**, **5**, and **6**, which had β values of 49, 159, and 128 cm^4/statvolt, respectively. The addition of only one double bond between the imidazole and 1,4-phenylene π linker, as in compound **5**, resulted in a tripling of the NLO response. On the contrary, its replacement with a less-polarizable triple bond in compound **6** led to a decrease in hyperpolarizability by 31 cm^4/statvolt. It should be noted that the introduction of the olefinic subunit between the imidazole acceptor and the central π linker improved the polarizability more significantly than its connection to the ferrocene donor (cf. β values for compounds **4**, **5**, and **7**). This fact can be further demonstrated by comparing chromophores **10** and **12**, for which the highest hyperpolarizabilities were calculated to be 393 and 396 cm^4/statvolt, respectively. Although chromophore **12** possesses a twisted biphenyl central π linker, its connection to the imidazole acceptor through the olefinic subunit caused a significant enhancement in its β value compared to chromophores **13**–**15**, which featured larger π linkers.

Charge transfer in these studied compounds was also demonstrated by a comparison of the DFT dipole moments in the ground and excited states. In Table 3, the ground-state dipole moment of each compound is compared to their dipole moment in the vertically excited state, that is, with excited electrons, but still in an unrelaxed ground-state geometry. The largest increases in dipole moment were demonstrated by compounds **5**, **10**, **11**, and **13**, which were also those chromophores that gave the strongest experimental NLO responses (Table 3).

The calculated NLO data were preliminary verified by measuring the second harmonic generation (SHG) values of these compounds (Table 3). The SHG experiment was carried out at 1064 nm, with the NLO-phore embedded into a polycarbonate matrix (7.7–8.5 %).[29] Only the values for the chromophores that delivered clear SHG signal are

shown. Although these values (Table 3) should be interpreted with caution, they showed the same trend as the calculated values, with the highest NLO response observed for chromophore **10**.

Conclusions

A series of fifteen push–pull molecules with a ferrocene donor, a 4,5-dicyanoimidazole acceptor, and systematically varied and enlarged π linkers were prepared by using cross-coupling reactions. These inorganic–organic hybrid materials were investigated by X-ray analysis, electrochemistry, electronic absorption spectroscopy, DFT calculations, and SHG measurements. The RTG data of five selected compounds revealed substantial differences in the spatial arrangement of the π linkers that were used in the particular chromophores. 1,4-Phenylene subunits that were appended directly onto either the donor or the acceptor were forced out of the main plane of the chromophore, which resulted in diminished ICT. On the contrary, the introduction of additional olefinic or acetylenic subunits led to improved D–A conjugation. The electrochemical data were dependent on the structure and length of the π linker: Its extension and planarization caused a substantial decrease in the HOMO–LUMO gap, whilst the smallest difference between the first oxidation and reduction potentials was observed for chromophore **10**. The absorption spectra showed two clearly distinguishable HE and LE bands; whereas the position of the HE band was strongly affected by the character of the π linker, the LE transition was pronounced for chromophores with planar and polarizable π linkers, such as that in compound **10**. In addition to the experimental data, chromophores **1**–**15** were thoroughly investigated by using (TD)DFT calculations; the absorption spectra, HOMO/LUMO levels, and second-order polarizabilities (β) ($-2\omega,\omega,\omega$) of these compounds were calculated. Both the predicted spectra and the HOMO/LUMO levels for all of the chromophores correlated reasonably well with the experimental data. Moreover, the calculated β ($-2\omega,\omega,\omega$) values exactly mirrored the observed trends in all of the aforementioned analytical measurements that were used to determine the extent of D–A interactions, with the highest second-order polarizability both predicted and measured for chromophores **10**/**12**.

With the same ferrocene donor and imidazole acceptor in all of the tested compounds, all of the changes in the measured data were attributed to the structure, electronic nature, and spatial arrangement of the π linker. Systematic variation and extension of the π linker allowed for a detailed study of any structure–property relationships in these compounds and a tailoring of the π linker for second-order nonlinear optics. The most important structural features that affect the ground-state D–A conjugation (ICT) and respective nonlinear optical properties of these inorganic–organic hybrid D–π–A systems (**1**–**15**) are 1) The presence of olefinic/acetylenic subunits; 2) the length of the π linker; and 3) the spatial arrangement (planarity) of the π linker. Hence, considering all of the measured data, chromophores **10**/**12** can be regarded as very attractive candidates for device integration.

Experimental Section

General

Starting materials **16**,[16] **17**,[17] **18**,[21] and **19**[5e] were synthesized according to literature procedures. The synthesis and spectroscopic characterization of ferrocene-substituted precursors **20**–**29** are found in the Supporting Information. Column chromatography was carried out on silica gel 60 (particle size: 0.040–0.063 mm, 230–400 mesh; Merck) with commercially available solvents. Thin-layer chromatography (TLC) was conducted on aluminum sheets that were coated with silica gel 60 F254 (Merck) under visualization by a UV lamp (254 or 360 nm). Melting points (m.p.) were measured on a Buchi B-540 melting-point apparatus in open capillaries and are uncorrected. ^{1}H and ^{13}C NMR spectra were recorded at 400 and 100 MHz, respectively, on a Bruker AVANCE 400 instrument at 25 °C. Chemical shifts are reported in ppm relative to $SiMe_4$. The residual solvent signal in the ^{1}H and ^{13}C NMR spectra was used as an internal reference ($CDCl_3$: $\delta = 7.25$ and 77.23 ppm). Apparent resonance multiplicities are described as s (singlet), br s (broad singlet), d (doublet), dd (doublet of doublet), and m (multiplet). IR spectra were recorded on a Perkin–Elmer FTIR Spectrum BX spectrometer. Mass spectra were measured on a GCMS, which was comprised of an Agilent Technologies 6890N gas chromatograph that was equipped with a 5973 Network MS detector (EI 70 eV, mass range: 33–550 Da) or on an LC-MS Micromass Quattro Micro API (Waters) instrument with a direct input (ESI, MeOH, mass range: 200–1000 Da). Elemental analysis was performed on an EA 1108 Fisons instrument. UV/Vis spectra were recorded on a Hewlett–Packard 8453 spectrophotometer in CH_2Cl_2.

General Method for the Suzuki–Miyaura Cross-Coupling Reaction (Method A)

Compound **16**, **18**, or 4-bromophenylferrocene (1.0 mmol) and an appropriate boronic acid or its pinacol ester (1.0 mmol) were dissolved in THF (16 mL) and water (4 mL). Argon was bubbled through the solution for 10 min, whereupon $[PdCl_2(PPh_3)_2]$ (35 mg, 0.05 mmol) and Na_2CO_3 (116 mg, 1.1 mmol) were added and the reaction mixture was stirred under an argon atmosphere at 80 °C for 5 h. The reaction was diluted with water and extracted with CH_2Cl_2 (2×100 mL), the combined organic extracts were dried (Na_2SO_4), and the solvents were evaporated in vacuo. The crude product was purified by column chromatography on silica gel (CH_2Cl_2).

General Method for the Heck Olefination Reaction (Method B)

Methylvinazene (**17**, 158 mg, 1.0 mmol), an appropriate bromo- or iodo derivative (1.0 mmol), and diisopropylethylamine (0.2 mL) were dissolved in dry DMF (5 mL). Argon was bubbled through the solution for 10 min, whereupon $[Pd\{P(tBu)_3\}_2]$ (25 mg, 0.05 mmol) was added and the reaction mixture was stirred under an argon atmosphere at 85 °C for 12 h. The reaction was diluted with water and extracted with CH_2Cl_2 (2× 100 mL), the combined organic extracts were dried (Na_2SO_4), and the solvents were evaporated in vacuo. The crude product was purified by column chromatography on silica gel (CH_2Cl_2).

General Method for the Sonogashira Cross-Coupling Reaction (Method C)

Compound **16** or **18** (1.0 mmol), an appropriate terminal acetylene, and diisopropylethylamine (1.0 mL) were dissolved in dry THF (20 mL). Argon was bubbled through the solution for 10 min, whereupon $[PdCl_2(PPh_3)_2]$ (35 mg, 0.05 mmol) and CuI (19 mg, 0.1 mmol) were added and the reaction mixture was stirred under an argon atmosphere at 25 °C for 2 h. The reaction was diluted with water and extracted with CH_2Cl_2 (2× 100 mL), the combined organic extracts were dried (Na_2SO_4), and the

solvents were evaporated in vacuo. The crude product was purified by column chromatography on silica gel (CH_2Cl_2).

*2-Ferrocenyl-1-methylimidazole-4,5-dicarbonitrile (**1**)*

The title compound was synthesized from compound **16** (211 mg, 1.0 mmol) and ferroceneboronic acid (230 mg, 1.0 mmol) according to general Method A. The solvent system was toluene (15 mL) and water (2 mL). The reaction was stirred under an argon atmosphere at 100 °C for 12 h. Yield: 66 mg (21 %); orange solid; R_f = 0.8 (CH_2Cl_2); m.p. 202–204 °C; ^{1}H NMR ($CDCl_3$, 400 MHz, 25 °C): δ = 3.91 (s, 3H; NCH_3), 4.21 (s, 5H; Cp), 4.50 (t, J = 2.0 Hz, 2H; Cp), 4.79 ppm (t, J = 2.0 Hz, 2H; Cp); ^{13}C NMR ($CDCl_3$, 100 MHz, 25 °C): δ = 34.3, 69.2, 70.2, 71.0, 77.4, 108.9, 112.1, 113.2, 122.4, 153.6 ppm; FTIR (HATR): $\tilde{\nu}$ = 2920, 2233, 1539, 1463, 1096, 1020, 818 cm^{-1}; MS (EI): m/z (%): 316 (100) [M]$^+$, 251 (20), 121 (21); elemental analysis calcd (%) for $C_{16}H_{12}FeN_4$: C 60.79, H 3.83, N 17.72; found: C 60.97, H 3.83, N 17.63.

*2-[(E)-2-Ferrocenylethenyl]-1-methylimidazole-4,5-dicarbonitrile (**2**)*

The title compound was synthesized from compound **17** (158 mg, 1.0 mmol) and iodoferrocene (308 mg, 1.0 mmol) according to general Method B. Yield: 150 mg (44 %); red solid; R_f = 0.6 (CH_2Cl_2); m.p. 289 °C (dec.); ^{1}H NMR ($CDCl_3$, 400 MHz, 25 °C): δ = 3.78 (s, 3H; NCH_3), 4.17 (s, 5H; Cp), 4.45 (t, J = 1.9 Hz, 2H; Cp), 4.51 (t, J = 1.9 Hz, 2H; Cp), 6.33 (d, J = 15.4 Hz,1H; CH), 7.69 ppm (d, J = 15.4 Hz, 1H; CH); ^{13}C NMR ($CDCl_3$, 100 MHz, 25 °C): δ = 32.6, 68.30, 69.9, 71.2, 79.8, 106.6, 109.0, 112.2, 112.2, 122.6, 141.8, 151.3 ppm; FTIR (HATR): $\tilde{\nu}$ = 2925, 2227, 1627, 1470, 1031, 968, 834, 812 cm^{-1}; MS (EI): m/z (%): 342 (48) [M]$^+$, 277 (100), 207 (12), 121 (15); elemental analysis calcd (%) for $C_{18}H_{14}FeN_4$: C 63.18, H 4.12, N 16.37; found: C 62.89, H 4.37, N 15.99.

*2-(2-Ferrocenylethynyl)-1-methylimidazole-4,5-dicarbonitrile (**3**)*

The title compound was synthesized from compound **16** (211 mg, 1.0 mmol) and ethynylferrocene (210 mg, 1.0 mmol) according to general Method C. Yield: 163 mg (48 %); orange solid; R_f = 0.6 (CH_2Cl_2); m.p. 232–235 °C; ^{1}H NMR ($CDCl_3$, 400 MHz, 25 °C): δ = 3.87 (s, 3H; NCH_3), 4.26 (s, 5H; Cp), 4.38 (t, J = 2.0 Hz, 2H; Cp), 4.60 ppm (t, J = 2.0 Hz, 2H; Cp); ^{13}C NMR ($CDCl_3$, 100 MHz, 25 °C): δ = 34.0, 60.4, 70.6, 70.6, 72.3, 72.5, 98.8, 108.1, 111.5, 112.4, 122.5, 137.5 ppm; FTIR (HATR): $\tilde{\nu}$ = 2921, 2217, 1734, 1466, 1101, 1028, 834, 815 cm^{-1}; MS (EI): m/z (%): 340 (100) [M]$^+$, 275 (10), 219 (8), 121 (35); elemental analysis calcd (%) for $C_{18}H_{12}FeN_4$: C 63.56, H 3.56, N 16.47; found: C 63.70, H 3.75, N 16.44.

*2-(2-Ferrocenylphenyl)-1-methylimidazole-4,5-dicarbonitrile (**4**)*

The title compound was synthesized from compounds **16** (211 mg, 1.0 mmol) and **25** (388 mg, 1.0 mmol) according to general Method A. Yield: 282 mg (72 %); orange solid; R_f = 0.8 (CH_2Cl_2); m.p. 213–216 °C; ^{1}H NMR ($CDCl_3$, 400 MHz, 25 °C): δ = 3.93 (s, 3H; NCH_3), 4.05 (s, 5H; Cp), 4.41 (t, J = 2.0 Hz, 2H; Cp), 4.70 (t, J = 2.0 Hz, 2H; Cp), 7.54 (d, J = 8.8 Hz, 2H; PhH), 7.59 ppm (d, J = 8.8 Hz, 2H; PhH); ^{13}C NMR ($CDCl_3$, 100 MHz, 25 °C): δ = 35.0, 67.0, 70.0, 70.1, 83.1, 108.7, 112.0, 114.1, 122.6, 124.0, 126.6, 129.2, 143.9, 152.9 ppm; FTIR (HATR): $\tilde{\nu}$ = 2921, 2230, 1610, 1465, 1101, 998, 837, 810 cm^{-1}; MS (EI): m/z (%): 392 (100) [M]$^+$, 287 (10), 196 (16), 121 (33); elemental analysis calcd (%) for $C_{22}H_{16}FeN_4$: C 67.37, H 4.11, N 14.28; found: C 67.74, H 4.31, N 14.56.

*2-[(E)-2-(4-Ferrocenylphenyl)ethenyl]-1-methylimidazole-4,5-dicarbonitrile (**5**)*

The title compound was synthesized from compound **17** (158 mg, 1.0 mmol) and 4-bromophenylferrocene (342 mg, 1.0 mmol) according to general Method B. Yield: 271 mg (65 %); red solid; R_f = 0.8 (CH_2Cl_2); m.p. 265–267 °C; ^{1}H NMR ($CDCl_3$, 400 MHz, 25 °C): δ = 3.84 (s, 3H; NCH_3), 4.04 (s, 5H; Cp), 4.38 (t, J = 2.0 Hz, 2H; Cp), 4.68 (t, J = 2.0 Hz, 2H; Cp), 6.73 (d, J = 15.6 Hz, 1H; CH), 7.45 (d, J = 8.8 Hz, 2H; PhH), 7.49 (d, J = 8.8 Hz, 2H; PhH), 7.80 ppm (d, J = 15.6 Hz, 1H; CH); ^{13}C NMR ($CDCl_3$, 100 MHz, 25 °C): δ = 32.8, 66.8, 69.9, 70.0, 83.9, 108.6, 108.8, 112.1, 112.7, 122.7, 126.6, 128.0, 132.3, 140.8, 142.6, 151.0 ppm; FTIR (HATR): $\tilde{\nu}$ = 2920, 2194, 1708, 1418, 1362, 1222, 818 cm^{-1}; MS (ESI): m/z: 418 [M]$^+$, 441 [M+23]$^+$, 859 [2M+23]$^+$, 1277 [3M+23]$^+$; elemental analysis calcd (%) for $C_{24}H_{18}FeN_4$: C 68.92, H 4.34, N 13.39; found: C 68.73, H 4.51, N 13.45.

*2-[(4-Ferrocenylphenyl)ethynyl]-1-methylimidazole-4,5-dicarbonitrile (**6**)*

The title compound was synthesized from compounds **16** (211 mg, 1.0 mmol) and **26** (286 mg, 1.0 mmol) according to general Method C. Yield: 129 mg (31 %); orange solid; R_f = 0.7 (CH_2Cl_2); m.p. 268–270 °C; ^{1}H NMR ($CDCl_3$, 400 MHz, 25 °C): δ = 3.94 (s, 3H; NCH_3), 4.04 (s, 5H; Cp), 4.40 (t, J = 2.0 Hz, 2H; Cp), 4.69 (t, J = 2.0 Hz, 2H; Cp), 7.49 ppm (br s, 4H; PhH); ^{13}C NMR ($CDCl_3$, 100 MHz, 25 °C): δ = 34.1, 67.0, 70.1, 70.2, 83.2, 98.0, 108.0, 111.4, 112.8, 116.3, 122.7, 126.3, 132.6, 137.3, 1143.6 ppm; FTIR (HATR): $\tilde{\nu}$ = 2919, 2212, 1710, 1416, 1361, 1222, 821 cm^{-1}; MS (ESI): m/z: 416 [M]$^+$, 439 [M+23]$^+$, 855 [2M+23]$^+$, 1271 [3M+23]$^+$; elemental analysis calcd (%) for $C_{24}H_{16}FeN_4$: C 69.25, H 3.87, N 13.46; found: C 69.46, H 4.01, N 13.20.

*2-{4-[(E)-Ferrocenylethenyl]phenyl}-1-methylimidazole-4,5-dicarbonitrile (**7**)*

The title compound was synthesized from compounds **18** (286 mg, 1.0 mmol) and **21** (338 mg, 1.0 mmol) according to general Method A. Yield: 171 mg (41 %); red solid; R_f = 0.6 (CH_2Cl_2); m.p. 218–221 °C; ^{1}H NMR ($CDCl_3$, 400 MHz, 25 °C): δ = 3.92 (s, 3H; NCH_3), 4.15 (s, 5H; Cp), 4.34 (t, J = 2.0 Hz, 2H; Cp), 4.49 (t, J = 2.0 Hz, 2H; Cp), 6.70 (d, J = 16.0 Hz, 1H; CH), 7.01 (d, J = 16.0 Hz, 1H; CH), 7.55 (d, J = 8.8 Hz, 2H; PhH), 7.59 ppm (d, J = 8.8 Hz, 2H; PhH); ^{13}C NMR ($CDCl_3$, 100 MHz, 25 °C): δ = 35.0, 67. 4, 69.6, 69.9, 82.5, 108.7, 112.0, 114.2, 122.5, 124.4, 124.8, 126.4, 129.5, 130.7, 141.1, 152.7 ppm; FTIR (HATR): $\tilde{\nu}$ = 2970, 2235, 1712, 1445, 1365, 1219, 809 cm^{-1}; MS (ESI): m/z: 418 [M]$^+$, 441 [M+23]$^+$, 859 [2M+23]$^+$, 1277 [3M+23]$^+$; elemental analysis calcd (%) for $C_{24}H_{18}FeN_4$: C 68.92, H 4.34, N 13.39; found: C 69.25, H 4.52, N 13.29.

*2-[4-(Ferrocenylethynyl)phenyl]-1-methylimidazole-4,5-dicarbonitrile (**8**)*

The title compound was synthesized from compounds **16** (211 mg, 1.0 mmol) and **22** (412 mg, 1.0 mmol) according to general Method A. Yield: 256 mg (62 %); orange solid; R_f = 0.7 (CH_2Cl_2); m.p. 203–206 °C; ^{1}H NMR ($CDCl_3$, 400 MHz, 25 °C): δ = 3.89 (s, 3H; NCH_3), 4.25 (s, 5H; Cp), 4.28 (t, J = 1.9 Hz, 2H; Cp), 4.52 (t, J = 1.9 Hz, 2H; Cp), 7.57–7.62 ppm (m, 4H; PhH); ^{13}C NMR ($CDCl_3$, 100 MHz, 25 °C): δ = 35.0, 64.3, 69.5, 70.3, 71.8, 84.9, 92.6, 108.5, 111.9, 114.3, 122.5, 125.6, 127.5, 129.1, 132.0, 152.2 ppm; FTIR (HATR): $\tilde{\nu}$ = 2919, 2202, 1713, 1421, 1360, 1222, 820 cm^{-1}; MS (ESI): m/z: 416 [M]$^+$, 439 [M+23]$^+$, 855 [2M+23]$^+$, 1271 [3M+23]$^+$; elemental analysis calcd (%) for $C_{24}H_{16}FeN_4$: C 69.25, H 3.87, N 13.46; found: C 69.68, H 4.03, N 13.23.

*2-(4′-Ferrocenylbiphenyl-4-yl)-1-methylimidazole-4,5-dicarbonitrile (**9**)*

The title compound was synthesized from compounds **18** (286 mg, 1.0 mmol) and **25** (388 mg, 1.0 mmol) according to general Method A. Yield: 238 mg (51 %); orange solid; R_f = 0.5 (CH_2Cl_2); m.p. 276 °C (dec.); ^{1}H NMR ($CDCl_3$, 400 MHz, 25 °C): δ = 3.96 (s, 3H; NCH_3), 4.07 (s, 5H; Cp), 4.36 (t, J = 2.0 Hz, 2H; Cp), 4.69 (t, J = 1.9 Hz, 2H; Cp), 7.55–7.60 (m, 4H; PhH), 7.71 (d, J = 8.8 Hz, 2H; PhH), 7.78 ppm (d, J = 8.8 Hz, 2H; PhH); ^{13}C NMR ($CDCl_3$, 100 MHz, 25 °C): δ = 35.0, 66.8, 69.6, 69.9, 84.5, 108.7, 112.0, 114.3, 122.6, 125.5, 126.9, 127.3, 127.6, 129.7, 136.9, 140.2, 144.1, 152.6 ppm; FTIR (HATR): $\tilde{\nu}$ = 2920, 2235, 1710, 1440, 1361, 1222, 823 cm^{-1}; MS (ESI): m/z: 468 [M]$^+$, 491 [M+23]$^+$, 959 [2M+23]$^+$, 1427 [3M+23]$^+$; elemental analysis calcd (%) for $C_{28}H_{20}FeN_4$: C 71.81, H 4.30, N 11.96; found: C 71.68, H 4.39, N 12.01.

*2-[(E)-2-{4-[(E)-Ferrocenylethenyl]phenyl}ethenyl]-1-methylimidazole-4,5-dicarbonitrile (**10**)*

The title compound was synthesized from compounds **17** (158 mg, 1.0 mmol) and **29** (366 mg, 1.0 mmol) according to general Method B. Yield: 195 mg (44 %); red solid; R_f = 0.5 (CH_2Cl_2); m.p. 294 °C (dec.); ^{1}H NMR ($CDCl_3$, 400 MHz, 25 °C): δ = 3.87 (s, 3H; NCH_3), 4.14 (s, 5H; Cp), 4.32 (t, J = 2.0 Hz, 2H; Cp), 4.48 (t, J = 1.9 Hz, 2H; Cp), 6.69 (d, J = 16.0 Hz, 1H; CH), 6.77 (d, J = 15.6 Hz, 1H; CH), 6.96 (d, J = 16.0 Hz, 1H; CH), 7.45 (d, J = 8.4 Hz, 2H; PhH), 7.51 (d, J = 8.4 Hz, 2H; PhH),

7.81 ppm (d, $J=15.6$ Hz, 1H; C*H*); ^{13}C NMR ($CDCl_3$, 100 MHz, 25 °C): $\delta=32.8$, 67.3, 69.5, 69.7, 82.9, 108.8, 108.8, 112.0, 112.8, 122.8, 125.1, 126.5, 128.3, 129.4, 133.1, 140.2, 140.6, 151.0 ppm; FTIR (HATR): $\tilde{\nu}=$ 2925, 2229, 1625, 1592, 1459, 1174, 959, 828, 810 cm^{-1}; MS (ESI): *m*/*z*: 469 $[M+23]^+$, 911 $[2M+23]^+$, 1355 $[3M+23]^+$; elemental analysis calcd (%) for $C_{26}H_{20}FeN_4$: C 70.28, H 4.54, N 12.61; found: C 70.54, H 4.62, N 12.51.

*2-[(E)-2-[4-(Ferrocenylethynyl)phenyl]ethenyl]-1-methylimidazole-4,5-dicarbonitrile (**11**)*

The title compound was synthesized from compounds **16** (211 mg, 1.0 mmol) and **24** (438 mg, 1.0 mmol) according to general Method A. Yield: 243 mg (55 %); orange solid; $R_f=0.5$ (CH_2Cl_2); m.p. 212–214 °C; ^{1}H NMR ($CDCl_3$, 400 MHz, 25 °C): $\delta=3.85$ (s, 3H; NCH_3), 4.24 (s, 5H; Cp), 4.26 (s, 2H; Cp), 4.50 (s, 2H; Cp), 6.78 (d, $J=15.6$ Hz, 1H; C*H*), 7.50 (br s, 4H; Ph*H*), 7.80 ppm (d, $J=15.6$ Hz, 1H; C*H*); ^{13}C NMR ($CDCl_3$, 100 MHz, 25 °C): $\delta=32.8$, 64.8, 69.4, 70.2, 71.7, 85. 7, 91.7, 108.7, 110.1, 112.0, 112.9, 122.7, 126.1, 127.7, 132.1, 133.8, 140.8, 150.6 ppm; FTIR (HATR): $\tilde{\nu}=2925$, 2227, 1724, 1605, 1357, 1219, 972, 823 cm^{-1}; MS (ESI): *m*/*z*: 442 $[M]^+$, 465 $[M+23]^+$, 907 $[2M+23]^+$, 1349 $[M+23]^+$; elemental analysis calcd (%) for $C_{26}H_{18}FeN_4$: C 70.60, H 4.10, N 12.67; found: C 70.89, H 4.29, N 12.81.

*2-[(E)-2-(4′-Ferrocenylbiphenyl-4-yl)ethenyl]-1-methylimidazole-4,5-dicarbonitrile (**12**)*

The title compound was synthesized from 4-bromophenylferrocene (342 mg, 1.0 mmol) and compound **19** (360 mg, 1.0 mmol) according to general Method A. Yield: 341 mg (69 %); orange solid; $R_f=0.4$ (CH_2Cl_2); m.p. 320 °C (dec.); ^{1}H NMR ($CDCl_3$, 400 MHz, 25 °C): $\delta=3.88$ (s, 3H; NCH_3), 4.06 (s, 5H; Cp), 4.35 (t, $J=2.0$ Hz, 2H; Cp), 4.51 (t, $J=$ 2.0 Hz, 2H; Cp), 6.82 (d, $J=15.6$ Hz, 1H; C*H*), 7.55 (br s, 4H; Ph*H*), 7.63 (d, $J=8.4$ Hz, 2H; Ph*H*), 7.67 (d, $J=8.4$ Hz, 2H; Ph*H*), 7.88 ppm (d, $J=15.6$ Hz, 1H; C*H*); ^{13}C NMR ($CDCl_3$, 100 MHz, 25 °C): $\delta=32.8$, 66.8, 69.4, 69.9, 84.8, 108.7, 109.6, 112.1, 112. 9, 122.8, 126.8, 127.1, 127.5, 128.4, 133.6, 137.4, 139.7, 140.6, 143.0, 150.8 ppm; FTIR (HATR): $\tilde{\nu}=2925$, 2227, 1737, 1604, 1357, 1221, 966, 819 cm^{-1}; MS (ESI): *m*/*z*: 494 $[M]^+$, 517 $[M+23]^+$, 1011 $[2M+23]^+$, 1505 $[3M+23]^+$; elemental analysis calcd (%) for $C_{30}H_{22}FeN_4$: C 72.89, H 4.49, N 11.33; found: C 73.19, H 4.72, N 11.37.

*2-[4-[(E)-2-(4-Ferrocenylphenyl)ethenyl]phenyl]-1-methylimidazole-4,5-dicarbonitrile (**13**)*

The title compound was synthesized from compounds **18** (286 mg, 1.0 mmol) and **27** (414 mg, 1.0 mmol) according to general Method A. Yield: 321 mg (65 %); orange solid. $R_f=0.4$ (CH_2Cl_2); m.p. 229–231 °C; ^{1}H NMR ($CDCl_3$, 400 MHz, 25 °C): $\delta=3.94$ (s, 3H; NCH_3), 4.05 (s, 5H; Cp), 4.35 (t, $J=1.6$ Hz, 2H; Cp), 4.68 (t, $J=1.6$ Hz, 2H; Cp), 7.12 (d, $J=$ 16.4 Hz, 1H; C*H*), 7.21 (d, $J=16.4$ Hz, 1H; C*H*), 7.45–7.51 (m, 4H; Ph*H*), 7.62–7.68 ppm (m, 4H; Ph*H*); ^{13}C NMR ($CDCl_3$, 100 MHz, 25 °C): $\delta=35.0$, 66.7, 69.5, 69.9, 84.7, 108.7, 112.0, 114.2, 122.6, 125.5, 126.1, 126.5, 127.1, 127.1, 129.6, 131.6, 134.3, 140.2, 140.8, 152.5 ppm; FTIR (HATR): $\tilde{\nu}=2925$, 2238, 1722, 1595, 1358, 1222, 969, 840, 827 cm^{-1}; MS (ESI): *m*/*z*: 494 $[M]^+$, 517 $[M+23]^+$, 1011 $[2M+23]^+$, 1505 $[3M+23]^+$; elemental analysis calcd (%) for $C_{30}H_{22}FeN_4$: C 72.89, H 4.49, N 11.33; found: C 73.15, H 4.57, N 11.26.

*2-[4-[4-(Ferrocenylphenyl)ethynyl]phenyl]-1-methylimidazole-4,5-dicarbonitrile (**14**)*

The title compound was synthesized from compounds **18** (286 mg, 1.0 mmol) and **26** (286 mg, 1.0 mmol) according to general Method C. Yield: 202 mg (41 %); orange solid. $R_f=0.5$ (CH_2Cl_2); m.p. 236–239 °C; ^{1}H NMR ($CDCl_3$, 400 MHz, 25 °C): $\delta=3.93$ (s, 3H; NCH_3), 4.04 (s, 5H; Cp), 4.37 (t, $J=1.6$ Hz, 2H; Cp), 4.67 (t, $J=1.6$ Hz, 2H; Cp), 7.46 (s, 4H; Ph*H*), 7.63 (d, $J=8.4$ Hz, 2H; Ph*H*), 7.63 ppm (d, $J=8.4$ Hz, 2H; Ph*H*); ^{13}C NMR ($CDCl_3$, 100 MHz, 25 °C): $\delta=35.0$, 66.8, 69.8, 70.0, 84.1, 88.3, 93.4, 108.5, 111.8, 114.4, 119.6, 122.6, 126.1, 126.2, 127.0, 129.2, 132.0, 132.3, 141.1, 152.1 ppm; FTIR (HATR): $\tilde{\nu}=2970$, 2239, 1711, 1443, 1359, 1221, 998, 839, 826 cm^{-1}; MS (ESI): *m*/*z*: 492 $[M]^+$, 515 $[M+23]^+$, 1007 $[2M+23]^+$, 1499 $[3M+23]^+$; elemental analysis calcd (%) for $C_{30}H_{20}FeN_4$: C 73.18, H 4.09, N 11.38; found: C 72.75, H 4.33, N 11.26.

*2-(4″-Ferrocenyl-1,1′:4′,1″-terphenyl-4-yl)-1-methylimidazole-4,5-dicarbonitrile (**15**)*

The title compound was synthesized from compounds **18** (286 mg, 1.0 mmol) and **28** (464 mg, 1.0 mmol) according to general Method A. Yield: 277 mg (51 %); orange solid. $R_f=0.4$ (CH_2Cl_2); m.p. 315–318 °C; ^{1}H NMR ($CDCl_3$, 400 MHz, 25 °C): $\delta=3.96$ (s, 3H; NCH_3), 4.07 (s, 5H; Cp), 4.35 (s, 2H; Cp), 4.67 (s, 2H; Cp), 7.57 (s, 4H; Ph*H*), 7.72 (d, $J=$ 5.6 Hz, 6H; Ph*H*), 7.82 ppm (d, $J=7.6$ Hz, 2H; Ph*H*); ^{13}C NMR ($CDCl_3$, 100 MHz, 25 °C): $\delta=35.0$, 66.8, 69.4, 69.9, 84.9, 108.7, 111.9, 114.3, 122.6, 125.8, 126.8, 127.1, 127.6, 127.8, 127.8, 129.7, 137.8, 138.2, 139.3, 141.2, 143.8, 152.5 ppm; FTIR (HATR): $\tilde{\nu}=2970$, 2243, 1712, 1435, 1362, 1222, 1001, 821 cm^{-1}; MS (ESI): *m*/*z*: 544 $[M]^+$, 567 $[M+23]^+$, 1111 $[2M+23]^+$, 1655 $[3M+23]^+$; elemental analysis calcd (%) for $C_{34}H_{24}FeN_4$: C 75.01, H 4.44, N 10.29; found: C 75.02, H 4.65, N 10.27.

Acknowledgements

This research was supported by the Czech Science Foundation (P106/12/0392) and by a Polish NCN grant (NCN204 345740). Calculations were carried out at the Wroclaw Centre for Networking and Supercomputing (http://www.wcss.wroc.pl; grant no. 135). The COST-CMTS Action CM1002 "COnvergent Distributed Environment for Computational Spectroscopy (CoDECS)" is also acknowledged.

[1] a) Special issue on "Organic Electronics and Optoelectronics" (Eds.: S. R. Forrest, M. E. Thompson), *Chem. Rev.* **2007**, *107*, 923–1386; b) Special issue on "Materials for Electronics" (Eds.: R. D. Miller, E. A. Chandross), *Chem. Rev.* **2010**, *110*, 1–574; c) Special issue on "Organic Photovoltaics" (Eds.: J. L. Brédas, J. R. Durrant), *Acc. Chem. Res.* **2009**, *42*, 1689–1857; d) C. Li, M. Liu, N. G. Pschirer, M. Baumgarten, K. Müllen, *Chem. Rev.* **2010**, *110*, 6817–6855; e) Special issue on "Molecular conductors" (Ed.: P. Batail), *Chem. Rev.* **2004**, *104*, 4887–5782; f) Y. Ohmori, *Laser Photonics Rev.* **2009**, *4*, 300–310; g) B. J. Coe, *Chem. Eur. J.* **1999**, *5*, 2464–2471.

[2] a) P. N. Prasad, D. J. Williams, *Introduction to Nonlinear Optical Effects in Molecules&Polymers*, Wiley, New York, **1991**; b) M. Kivala, F. Diederich, *Acc. Chem. Res.* **2009**, *42*, 235–248; c) L. R. Dalton, *J. Phys. Condens. Matter* **2003**, *15*, R897–R934; d) F. Bureš, W. B. Schweizer, J. C. May, C. Boudon, J.-P. Gisselbrecht, M. Gross, I. Biaggio, F. Diederich, *Chem. Eur. J.* **2007**, *13*, 5378–5387; e) J.-M. Raimundo, P. Blanchard, N. Gallego-Planas, N. Mercier, I. Ledoux-Rak, R. Hierle, J. Roncali, *J. Org. Chem.* **2002**, *67*, 205–218.

[3] a) M. G. Kuzyk, *J. Mater. Chem.* **2009**, *19*, 7444–7465; b) J. Y. Lee, K. S. Kim, B. J. Mhin, *J. Chem. Phys.* **2001**, *115*, 9484–9489; c) T. Le Bahers, C. Adamo, I. Ciofini, *J. Chem. Theory Comput.* **2011**, *7*, 2498–2506; d) J. C. May, I. Biaggio, F. Bureš, F. Diederich, *Appl. Phys. Lett.* **2007**, *90*, 251106; e) S.-I. Kato, M. Kivala, W. B. Schweizer, C. Boudon, J.-P. Gisselbrecht, F. Diederich, *Chem. Eur. J.* **2009**, *15*, 8687–8691; f) F. Bureš, O. Pytela, M. Kivala, F. Diederich, *J. Phys. Org. Chem.* **2011**, *24*, 274–281.

[4] a) G. A. Lindsay, *Second-Order Nonlinear Optical Polymers* in *Polymers for Second-Order Nonlinear Optics* (Eds.: G. A. Lindsay, K. D. Singer), American Chemical Society, Washington, DC, **1995**; b) Z. Li, Q. Li, J. Qin, *Polym. Chem.* **2011**, *2*, 2723–2740; c) T. Kolev, I. V. Kityk, J. Ebothe, B. Sahraoui, *Chem. Phys. Lett.* **2007**, *443*, 309–312.

[5] a) For a recent review, see: J. Kulhánek, F. Bureš, *Beilstein J. Org. Chem.* **2012**, *8*, 25–49; b) J. Kulhánek, F. Bureš, O. Pytela, T. Mikysek, J. Ludvík, A. Růžička, *Dyes Pigm.* **2010**, *85*, 57–65; c) J. Kulhánek, F. Bureš, A. Wojciechowski, M. Makowska-Janusik, E. Gondek, I. V. Kityk, *J. Phys. Chem. A* **2010**, *114*, 9440–9446; d) A. Plaquet, B. Champagne, J. Kulhánek, F. Bureš, E. Bogdan, F. Castet, F. Ducasse, V. Rodriguez, *ChemPhysChem* **2011**, *12*, 3245–3252; e) J.

Kulhánek, F. Bureš, O. Pytela, T. Mikysek, J. Ludvík, *Chem. Asian J.* **2011**, *6*, 1604–1612.
[6] a) I. D. L. Albert, T. J. Marks, M. A. Ratner, *J. Am. Chem. Soc.* **1997**, *119*, 6575–6582; b) C. R. Moylan, B. J. McNelis, L. C. Nathan, M. A. Marques, E. L. Hermstad, B. A. Brichler, *J. Org. Chem.* **2004**, *69*, 8239–8243.
[7] For recent reviews on ferrocene materials, see: a) W. A. Amer, L. Wang, A. M. Amin, L. Ma, H. Yu, *J. Inorg. Organomet. Polym.* **2010**, *20*, 605–615; b) P. Debroy, S. Roy, *Coord. Chem. Rev.* **2007**, *251*, 203–221; c) G. R. Whittell, I. Manners, *Adv. Mater.* **2007**, *19*, 3439–3468; d) R. D. A. Hudson, *J. Organomet. Chem.* **2001**, *637–639*, 47–69; e) R. Horikoshi, T. Mochida, *Eur. J. Inorg. Chem.* **2010**, 5355–5371; f) V. Mamane, *Mini-Rev. Org. Chem.* **2008**, *5*, 303–312.
[8] a) M. F. R. Fouda, M. M. Abd-Elzaher, R. A. Abdelsamaia, A. A. Labib, *Appl. Organomet. Chem.* **2007**, *21*, 613–625; b) D. R. van Staveren, N. Metzler-Nolte, *Chem. Rev.* **2004**, *104*, 5931–5985.
[9] M. L. H. Green, S. R. Marder, M. E. Thompson, J. A. Bandy, D. Bloor, P. V. Kolinksy, R. J. Jones, *Nature* **1987**, *330*, 360–362.
[10] a) N. J. Long, *Angew. Chem.* **1995**, *107*, 37–56; *Angew. Chem. Int. Ed. Engl.* **1995**, *34*, 21–38; b) H. S. Nalwa, *Appl. Organomet. Chem.* **1991**, *5*, 349–377.
[11] a) M. M. Oliva, J. Casado, M. M. M. Raposo, A. M. C. Fonseca, H. Hartman, V. Hernández, J. T. L. Navarrete, *J. Org. Chem.* **2006**, *71*, 7509–7520; b) Y. Liao, B. E. Eichinger, K. A. Firestone, M. Haller, J. Luo, W. Kaminsky, J. B. Benedict, P. J. Reid, A. K.-Y. Jen, L. R. Dalton, B. H. Robinson, *J. Am. Chem. Soc.* **2005**, *127*, 2758–2766; c) C. J. McAdam, B. H. Robinson, J. Simpson, T. Tagg, *Organometallics* **2010**, *29*, 2474–2483; d) N. Tsuboya, M. Lamrani, R. Hamasaki, M. Ito, M. Mitsuishi, T. Miyashita, Y. Yamamoto, *J. Mater. Chem.* **2002**, *12*, 2701–2705; e) T. L. Kinnibrugh, S. Salman, Y. A. Getmanenko, V. Coropceanu, W. W. Perter III., T. V. Timofeeva, A. J. Matzger, J.-C. Brédas, S. R. Marder, S. Barlow, *Organometallics* **2009**, *28*, 1350–1357; f) I. Janowska, J. Zakrzewski, K. Nakatani, J. A. Delaire, M. Palusiak, M. Walak, H. Scholl, *J. Organomet. Chem.* **2003**, *675*, 35–41; g) I. Janowska, J. Zakrzewski, K. Nakatani, M. Palusiak, M. Walak, H. Scholl, *J. Organomet. Chem.* **2006**, *691*, 323–330; h) X.-B. Zhang, J.-K. Feng, A.-M. Ren, C.-C. Sun, *J. Phys. Chem. A* **2006**, *110*, 12222–12230; i) S. Barlow, H. E. Bunting, C. Ringham, J. C. Green, G. U. Bublitz, S. G. Boxer, J. W. Perry, S. R. Marder, *J. Am. Chem. Soc.* **1999**, *121*, 3715–3723; j) G. G. A. Balavoine, J.-C. Daran, G. Iftime, P. G. Lacroix, E. Manoury, J. A. Delaire, I. Maltey-Fantom, K. Nakatani, S. Di Bella, *Organometallics* **1999**, *18*, 21–29; k) E. Stankovic, S. Toma, R. Van Boxel, I. Asselberghs, A. Persoons, *J. Organomet. Chem.* **2001**, *637–639*, 426–434.
[12] S.-G. Liu, I. Pérez, N. Martín, L. Echegoyen, *J. Org. Chem.* **2000**, *65*, 9092–9102.
[13] a) B. J. Coe, R. J. Docherty, S. P. Foxon, E. C. Harper, M. Helliwell, J. Raftery, K. Clays, E. Franz, B. S. Brunschwig, *Organometallics* **2009**, *28*, 6880–6892; b) K. Roque, F. Barangé, G. G. A. Balavoine, J.-C. Daran, P. G. Lacroix, E. Manoury, *J. Organomet. Chem.* **2001**, *637–639*, 531–537; c) D. A. Davies, J. Silver, G. Gross, P. Thomas, *J. Organomet. Chem.* **2001**, *631*, 59–66; d) C. Engtrakul, L. R. Sita, *Organometallics* **2008**, *27*, 927–937.
[14] a) G.-S. Huang, Y.-M. Liang, X.-L. Wu, W.-M. Liu, Y.-X. Ma, *Appl. Organomet. Chem.* **2003**, *17*, 706–710; b) S. K. Pal, A. Krishnan, P. K. Das, A. G. Samuelson, *J. Organomet. Chem.* **2000**, *604*, 248–259; c) A. Krishnan, S. K. Pal, P. Nandakumar, A. G. Samuelson, P. K. Das, *Chem. Phys.* **2001**, *265*, 313–322.
[15] I. Baumgardt, H. Butenschön, *Eur. J. Org. Chem.* **2010**, 1076–1087.
[16] a) D. W. Woodward, U. S. Patent 2534331, **1950**; b) J. F. O'Connell, J. Parquette, W. E. Yelle, W. Wang, H. Rapoport, *Synthesis* **1988**, 767–771.
[17] D. M. Johnson, P. G. Rasmussen, *Macromolecules* **2000**, *33*, 8597–8603.
[18] J. Kulhánek, F. Bureš, M. Ludwig, *Beilstein J. Org. Chem.* **2009**, *5*, No. 11.
[19] M. V. Makarov, V. P. Dyadchenko, M. Y. Antipin, *Russ. Chem. Bull. Int. Ed.* **2004**, *53*, 2768–2773.
[20] a) R. Y. C. Shin, P. Sonar, P. S. Siew, Z.-K. Chen, A. Sellinger, *J. Org. Chem.* **2009**, *74*, 3293–3298; b) R. Y. C. Shin, T. Kietzke, S. Sudhakar, A. Dodabalapur, Z.-K. Chen, A. Sellinger, *Chem. Mater.* **2007**, *19*, 1892–1894.
[21] a) P. S. Robertson, J. Vaughan, *J. Am. Chem. Soc.* **1958**, *80*, 2691–2693; b) G. A. Feldwick, L. R. Hatton, R. H. Hewett, B. L. Pedgrift, European Patent EP0269238, **1988**.
[22] a) J. L. Brédas, *Adv. Mater.* **1995**, *7*, 263–274; b) D. Jacquemin, A. Femenias, H. Chermette, J.-M. André, E. A. Perpète, *J. Phys. Chem. A* **2005**, *109*, 5734–5741.
[23] a) C. Dehu, F. Meyers, J. L. Brédas, *J. Am. Chem. Soc.* **1993**, *115*, 6198–6206; b) G. Bourhill, J. L. Brédas, L.-T. Cheng, S. R. Marder, F. Meyers, J. W. Perry, B. G. Tiemann, *J. Am. Chem. Soc.* **1994**, *116*, 2619–2620; c) J. L. Brédas, *J. Chem. Phys.* **1985**, *82*, 3808–3811; d) S. Yang, M. Kertesz, *J. Phys. Chem. A* **2006**, *110*, 9771–9774; e) D. Jacquemin, C. Adamo, *J. Chem. Theory Comput.* **2011**, *7*, 369–376.
[24] J. Corish, D. A. Morton-Blake, F. O'Donoghue, J. L. Baudour, F. Bénière, B. Toudic, *J. Mol. Struct.* **1995**, *358*, 29–38.
[25] M.-B. S. Kirketerp, M. Å. Petersen, M. Wanko, H. Zettergren, A. Rubio, M. B. Nielsen, S. B. Nielsen, *ChemPhysChem* **2010**, *11*, 2495–2498.
[26] A. A. Isse, A. Gennaro, *J. Phys. Chem. B* **2010**, *114*, 7894–7899.
[27] D. R. Kanis, M. A. Ratner, T. J. Marks, *J. Am. Chem. Soc.* **1992**, *114*, 10338–10357.
[28] J. Schäfer, M. Scheurer, B. Speiser, W. Kuźnik, I. V. Kityk, *Spectrochim. Acta Part A* **2012**, *95*, 193–198.
[29] M. Makowska-Janusik, I. V. Kityk, N. Gauthier, F. Paul, *J. Phys. Chem. C* **2007**, *111*, 12094–12099.

Received: October 16, 2012
Revised: November 5, 2012
Published online: November 27, 2012